Int. J. Heat Mass Transfer. Vol. 36, No. 1, pp. 101–117, 1993
Printed in Great Britain

0017–9310/93 $5.00 + 0.00
Pergamon Press Ltd

Thermogravitational and thermocapillary convection in a cavity containing two superposed immiscible liquid layers

Q. S. LIU, G. CHEN and B. ROUX

Institut de Mécanique des Fluides, Université d'Aix-Marseille II, UMR-34, 1, rue Honnorat, 13003 Marseille, France

(*Received* 12 *July* 1991 *and in final form* 25 *January* 1992)

Abstract—Steady thermogravitational and thermocapillary driven flows of two immiscible liquid layers is considered in the case of a cavity subjected to a horizontal temperature gradient. The Navier–Stokes equations with Boussinesq approximation are solved numerically by a finite difference method in a staggered grid. The pressure correction method is used to decouple the pressure calculation from that of the velocity. Convective patterns have been emphasized, numerically. They depend on property ratios of the two liquid layers and on depth fractions of the layers. Reduction of convection in the lower (encapsulated) layer can be achieved by a proper choice of the parameters. An asymptotic solution for the velocity is also presented for an infinite cavity ($A \to \infty$). It predicts the shape of the velocity profiles and determines the number of convective cells through the two layers. Both situations with rigid or with free top surface have been considered. This latter configuration is similar to that of an encapsulated crystal growth. The computations have been performed for flat interfaces, liquid–liquid and liquid–gas. Most of them have been limited to a cavity of aspect ratio $A = 2$ (length/height).

1. INTRODUCTION

THE FLOW in a two-layer system of immiscible fluids is known to exhibit phenomena which may not occur in one-layer systems; an example is the Bénard problem (horizontal layers heated from below). In the classical (one-layer) Bénard problem, the 'exchange of stabilities' hold and all the eigenvalues of the linearized problem are real. In a two-layer system, however, Renardy and Joseph [1] showed that both real and complex spectra exist. The two-layer system is much more complicated than the one-layer system due to continuity conditions that must be satisfied at the interface between two immiscible fluids. For the two-layer Bénard problem, attention has been paid to determine the onset of instabilities by means of linear stability analysis [2–7]. More recently, the flow of two immiscible fluids of different densities, in the case where a horizontal temperature gradient is applied, also received great consideration. This is due to the interest in the encapsulation technique for crystal growth, such as the encapsulated Czochralski (LEC) method [8] and the encapsulated floating zone technique for space processing of high-purity semiconductors. These two crystallization techniques involve multi-layer systems (two or three) subjected to both vertical and horizontal temperature gradients. Therefore, buoyancy driven convection (due to the density differences in the gravity field) and thermocapillary convection (induced by surface tension gradients along the non-isothermal interface due to the temperature dependency of the surface tension) may occur simultaneously.

For (horizontal) two-layer systems subjected to a horizontal temperature gradient, Villers and Platten [9] conducted an experimental study of the horizontal velocity profiles in each layer and temperature variation of interfacial tensions in a confined cavity of two immiscible liquids (water–heptanol). They found the dominant role of the interfacial tension effect. Crespo del Arco *et al.* [10] numerically studied pure thermocapillary convection in two immiscible fluids with $Pr_1 = 1$ and $Pr_2 = 0.01$ for $Ma \leqslant 120$; the flow in the lower layer of fluid can be significantly reduced by a proper choice of Marangoni numbers such that $Ma_1 = 2Ma_2$. Surprisingly there is not good agreement for low Ma with an analytical solution attributed due to Doi and Koster [11], except for the case $Ma_1 = 2Ma_2$.

The main objective of this research is to investigate the convective flow induced by buoyancy and interfacial forces in a rectangular cavity containing two layers of immiscible fluids. The interfacial tension gradients, $\partial\sigma/\partial T$, are created by a temperature difference imposed along the interface between two liquids and the liquid–gas interface. All the numerical results are obtained by a finite difference method. In this paper, the interface and the top surface are assumed to be flat. For the top surface two variants have been considered: either rigid or free. We show the influence of thermocapillary forces on the buoyancy-driven flow in each liquid layer. Also we give analytical expressions for the horizontal velocity in the two cases (rigid or free top surface), which can describe the types of convective pattern and predict some characteristics of the flow structure in the two-dimensional cavity.

NOMENCLATURE

A	aspect ratio, L/H
Bi	Biot number, $\eta_1 H/\lambda_1$
g	gravitational acceleration
Gr	Grashof number, $g\beta_2\delta T H^4/\nu_2^2$
H	height of the cavity
H_1	thickness of top layer
H_2	thickness of bottom layer
L	length of the cavity
Ma_i	Marangoni number for ith layer, $Pr\,Re_i$
Pr	Prandtl number, ν_2/α_2
Re_i	Reynolds number, $\gamma_i\delta T H^2/\nu_2\mu_2$
T	temperature
T_c	constant temperature at cold vertical wall
T_h	constant temperature at hot vertical wall
T_{ref}	reference temperature, $H\delta T$
ΔT	maximum temperature difference, $T_h - T_c$
U_{ref}	reference velocity, ν_2/H
h_i	dimensionless thickness, H_i/H
h^*	thickness ratio of two layers, H_1/H_2
p	dimensionless pressure
Pa_i	stream pattern parameters
u	dimensionless horizontal velocity component
v	dimensionless vertical velocity component
x	dimensionless horizontal coordinate
y	dimensionless vertical coordinate.

Greek symbols

α	thermal diffusivity
β	thermal expansion coefficient
γ	surface-tension temperature coefficient, $-\partial\sigma/\partial T$
δT	horizontal temperature gradient, $\Delta T/L$
η	heat transfer coefficient
θ	dimensionless temperature
θ_a	ambient temperature
λ	thermal conductivity
μ	dynamic viscosity
ν	kinematic viscosity
ρ	density
σ	surface tension
ϕ	any physical variable
Ψ	dimensionless streamfunction.

Subscript

i	physical properties of liquid i, $i = 1, 2$.

Superscript

*	physical property ratio of liquid 1 to liquid 2 (e.g. $\beta^* = \beta_1/\beta_2$).

2. PHYSICAL AND MATHEMATICAL MODEL

We consider a system of two immiscible viscous liquids, 1 (above) and 2 (below) (see Fig. 1), filling a rectangular cavity. The Cartesian x–y coordinate system contains the temperature gradient and the gravity acceleration, g, in the negative y direction. The thickness of layer 1 is H_1, and that for layer 2 is H_2, and the total thickness is H. The aspect ratio is $A = {}_1L/H$, where L is the length of the cavity. The thickness ratio of the two layers is $h^* = H_1/H_2$. In most of the present calculations, we will take $A = 2$ and $h^* = 1$.

The rectangular cavity has a rigid bottom wall, a liquid 1–liquid 2 interface and two types of boundary conditions for its upper surface: (i) rigid (denoted case A); and (ii) free (denoted case B). The vertical walls of the cavity are maintained at different constant temperatures: T_c and T_h ($T_h > T_c$). The horizontal walls are considered as perfectly conducting with a linear temperature profile. At the interface between the two layers, there exists a surface tension (mechanical

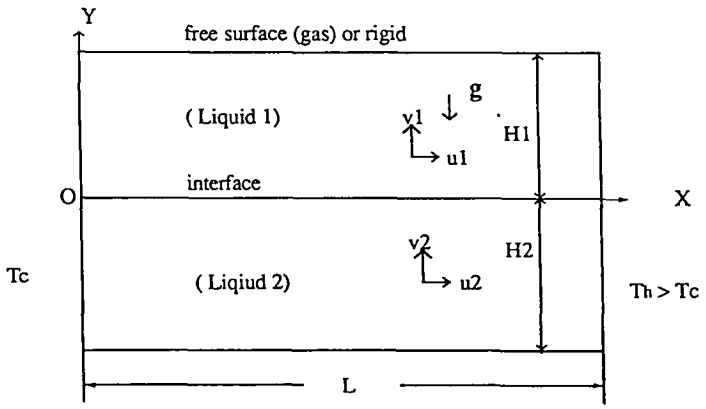

FIG. 1. Geometry and coordinate system of the physical model.

coupling), σ, which is assumed to linearly depend on the temperature

$$\sigma_2 = \sigma_{02} - \gamma_2(T_2 - T_0) \quad \text{with} \quad T_0 = (T_c + T_h)/2 \tag{1}$$

where σ_{02} is the interface tension between liquid 1 and liquid 2, and $\gamma_2 = -\partial\sigma_2/\partial T$ the rate of change of interface tension with temperature, at the temperature T_0. The two constants are related to material properties of both liquid 1 and liquid 2.

In case B, the top free surface is subjected to a surface tension varying linearly with temperature

$$\sigma_1 = \sigma_{01} - \gamma_1(T_1 - T_0) \tag{2}$$

where σ_{01} is the surface tension between liquid 1 and air, and $\gamma_1 = -\partial\sigma_1/\partial T$, at temperature T_0. In this paper, the free top surface is assumed to be flat; the liquid 1–liquid 2 interface is assumed to be undeformable and impervious. Therefore, heat is transferred through this interface only by the means of conduction. The density ρ_i, is directly connected to the temperature, through the Boussinesq approximation by

$$\rho_i = \rho_{0i}[1 - \beta_i(T_i - T_0)]. \tag{3}$$

Navier–Stokes and energy equations should be satisfied in each liquid layer. The governing equations can be written in the form of the primary dependent variables, that is U_i, p_i, T_i, with $U_i = (u_i, v_i)$, as

$$\frac{\partial u_i}{\partial x} + \frac{\partial v_i}{\partial y} = 0 \tag{4}$$

$$\frac{\partial u_i}{\partial t} + ZU_i\left[u_i\frac{\partial u_i}{\partial x} + v_i\frac{\partial u_i}{\partial y}\right] = -ZP_i\frac{\partial p_i}{\partial x} + ZD_i\left[\frac{\partial^2 u_i}{\partial x^2} + \frac{\partial^2 u_i}{\partial y^2}\right] \tag{5}$$

$$\frac{\partial v_i}{\partial t} + ZU_i\left[u_i\frac{\partial v_i}{\partial x} + v_i\frac{\partial v_i}{\partial y}\right] = -ZP_i\frac{\partial p_i}{\partial y} + ZD_i\left[\frac{\partial^2 v_i}{\partial x^2} + \frac{\partial^2 v_i}{\partial y^2}\right] + ZBT_i\theta \tag{6}$$

$$\frac{\partial \theta_i}{\partial t} + ZT_i\left[u_i\frac{\partial \theta_i}{\partial x} + v_i\frac{\partial \theta_i}{\partial y}\right] = TD_i\left[\frac{\partial^2 \theta_i}{\partial x^2} + \frac{\partial^2 \theta_i}{\partial y^2}\right] \tag{7}$$

where

$$\theta_i \equiv \frac{T_i - T_c}{T_{ref}}.$$

The constants in these dimensionless equations (5)–(7) depend on the choice of the scaling factors. We use $L_{ref} = H$, $U_{ref} = \nu_2/H$, and $t_{ref} = H^2/\nu_2$ as scaling factors for length, velocity and time, respectively. Temperature scale is taken as $T_{ref} = H\delta T$ ($\delta T = \Delta T/L$; $\Delta T = T_h - T_c$) and the reference pressure is taken as $p_{ref} = \rho_2 U_{ref}^2$, so the above coefficients are the following:

$$ZU_1 = 1; \quad ZP_1 = 1/\rho^*; \quad ZD_1 = \nu^*$$
$$ZBT_1 = Gr\,\beta^*; \quad ZT_1 = 1; \quad TD_1 = \alpha^*/Pr$$
$$ZU_2 = 1; \quad ZP_2 = 1; \quad ZD_2 = 1; \quad ZBT_2 = Gr$$
$$ZT_2 = 1; \quad TD_2 = 1/Pr.$$

Thus, the relations between two coefficient groups are the following:

$$ZU_1 = ZU_2; \quad ZP_1 = ZP_2/\rho^*$$
$$ZD_1 = \nu^* ZD_2; \quad ZBT_1 = \beta^* ZBT_2$$
$$ZT_1 = ZT_2; \quad TD_1 = \alpha^* TD_2.$$

The Grashof number, Gr, and the Prandtl number, Pr, entering in these coefficients are defined as corresponding to the lower layer:

$$Gr = \frac{g\beta_2(\delta T)H^4}{\nu_2^2}, \quad Pr = \frac{\nu_2}{\alpha_2}.$$

The dimensionless equations (4)–(7) are subjected to the following boundary conditions.

Kinematic boundary conditions

No-slip conditions are imposed at the rigid walls (bottom and two vertical walls):

$$u_2 = v_2 = 0, \quad \text{at} \quad y = -h_2 \,(\text{with } h_2 = H_2/H) \tag{8}$$

$$u_i = v_i = 0, \quad \text{at} \quad x = 0 \quad \text{and} \quad A. \tag{9}$$

For a rigid top surface (case A), we have

$$u_1 = v_1 = 0 \quad \text{at} \quad y = h_1 \,(\text{with } h_1 = H_1/H). \tag{10}$$

For a free top surface (case B), the contribution of thermocapillary forces in the convective flow enters the governing equation via the tangential-stress condition

$$\mu^*\frac{\partial u_1}{\partial y} = -Re_1\frac{\partial \theta_1}{\partial x}, \quad \text{at} \quad y = h_1 \tag{11}$$

where the surface Reynolds number Re_1, relative to liquid 1, is defined by

$$Re_1 = -\frac{\delta T H^2\,\partial\sigma_1/\partial T}{\mu_2\nu_2}$$

and the Marangoni number, relative to Re_1, is denoted by $Ma_1 = Pr\,Re_1$.

On the flat interface between the lower and upper layers, continuity of velocity must be satisfied

$$u_1 = u_2 \quad \text{and} \quad v_1 = v_2 = 0, \quad \text{at} \quad y = 0. \tag{12}$$

The balance of the stresses has to be satisfied too, and thus

$$\frac{\partial u_2}{\partial y} - \mu^*\frac{\partial u_1}{\partial y} = -Re_2\frac{\partial \theta}{\partial x}, \quad \text{at} \quad y = 0 \tag{13}$$

with

$$Re_2 = -\frac{H^2\delta T\,\partial\sigma_2/\partial T}{\mu_2\nu_2}$$

and the Marangoni number, relative to Re_2, is denoted by $Ma_2 = Pr\,Re_2$.

The Reynolds number Re_2 is relative to liquid 2, which characterizes the interfacial forces due to the temperature dependence of surface tension.

Thermal boundary conditions

The vertical walls are considered as isothermal

$$\theta_i = 0, \quad \text{at} \quad x = 0 \quad \text{and} \quad \theta_i = A, \quad \text{at} \quad x = A. \tag{14}$$

The horizontal top wall (for case A) and the lower wall are considered as perfectly conducting

$$\theta_i = x, \quad \text{at} \quad y = h_1 \quad \text{and} \quad y = -h_2. \tag{15}$$

On the free top surface (for case B)

$$\frac{\partial \theta_1}{\partial y} + Bi(\theta_1 - \theta_a) = 0 \tag{16}$$

where $Bi = \eta_1 H/\lambda_1$ is the Biot number and η_1 the heat transfer coefficient between liquid 1 and air, and θ_a the ambient dimensionless temperature. In the present work the numerical calculations were performed for $Bi = 0$.

At the liquid 1–liquid 2 interface, the continuity of temperature and the continuity of heat flux are represented, respectively, by

$$\theta_1 = \theta_2 \tag{17}$$

$$\lambda^* \frac{\partial \theta_1}{\partial y} = \frac{\partial \theta_2}{\partial y}. \tag{18}$$

3. ASYMPTOTIC SOLUTION AT FINITE H AND INFINITE L ($A \to \infty$)

3.1. *Rigid top surface (case A)*

The theoretical aspect of thermal convection in two superposed immiscible fluid layers in a rectangular cavity with differentially heated end walls has been studied by Villers and Platten [9]. They have given horizontal velocity and temperature profiles in case A as a function of the various parameters such as expansion coefficient, viscosity, depth of each layer, and the interfacial tension gradient along the interface, by considering that there is no vertical velocity component and that the horizontal velocity component is the same at any horizontal position. Another analytical investigation of thermal convection in a shallow cavity ($A \to \infty$) filled with two immiscible fluids is also performed by Wang *et al.* [12].

After taking into account the equilibrium conditions at the interface given by equation (13), and the mass conservation conditions, expressions for the horizontal velocity of each liquid layer in dimensionless form can be obtained. Upon the basis of the work in ref. [9], we may here give another expression of velocity profiles for case A and derive a new expression for the free top surface (case B).

For case A, the horizontal velocity is expressed in terms of a reduced coordinate y' as

$$u_1(y') = \frac{h_2^3 Q\alpha}{6Q\mu}\left[Gr\,y'^3 - \tfrac{3}{8}(4Gr + Pa_1)y'^2 + \tfrac{1}{2}(Pa_1 + Gr)y' - \tfrac{1}{8}Pa_1\right]$$

$$(0 \leqslant y' \leqslant 1), \quad \text{with} \quad y' = \frac{y}{h_1} \tag{19}$$

$$u_2(y') = \frac{h_2^3}{6}\left[Gr\,y'^3 + \tfrac{3}{8}(4Gr + Pa_2)y'^2 + \tfrac{1}{2}(Pa_2 + Gr)y' + \tfrac{1}{8}Pa_2\right]$$

$$(-1 \leqslant y' \leqslant 0), \quad \text{with} \quad y' = \frac{y}{h_2} \tag{20}$$

with

$$Pa_2 = -\frac{\left[Gr(1 - Q\alpha) + \dfrac{12Re_2}{h_2^2}\right]}{1 + Q\mu} \tag{21}$$

$$Pa_1 = -\frac{Q\mu}{Q\alpha} Pa_2. \tag{22}$$

Expressions (21) and (22) contain two parameters, $Q\alpha$ and $Q\mu$, introduced in ref. [9]

$$Q\alpha = \beta^* \rho^* (h^*)^2$$

$$Q\mu = \mu^*/h^*.$$

$Q\alpha$ represents the relative importance of the buoyancy between upper and lower layers, and $Q\mu$ is the ratio of the viscous forces. Pa_1 and Pa_2 are two dimensionless parameters which determine completely the shape of the velocity profiles in layers 1 and 2; they involve the ratios of the characteristic properties of two liquids and the effect of the interfacial forces. For these reasons, Pa_1 and Pa_2 will be referred to as 'stream pattern parameters' for the upper and lower layers, respectively. We can remark that the velocity (equations (19) and (20)) does not depend on Pr.

We compared the velocity profile (equations (19) and (20)) with the solution given by Villers and Platten [9]; (Fig. 5(c)) for $k = -Re_2/Gr = 0.35$ (e.g. $Gr = 1000$ and $Re_2 = -350$), $Q\alpha = 1.33$ and $Q\mu = 8.73$, $h_1 = 5.6$ and $h_2 = 3.7$. The form of the profile is the same (Fig. 2). Unfortunately, the velocity values cannot be compared as they are absent in Fig. 5(c).

In the absence of gravity, i.e. $Gr = 0$, the expressions of velocity profiles are quadratic with y, thus there exists only one convective cell in each layer induced by thermocapillary force. In the case $Gr \neq 0$, some characteristics of the velocity profiles may be found, from expressions (19) and (20):

(1) For the particular case where $Pa_1 = Pa_2 = 0$, the velocity at the interface is zero. Since the roots of $u_1(y')$ and $u_2(y')$ at which velocity is equal to zero are $y' = 1, 1/2, 0, -1/2$ and -1, there is only one cell in

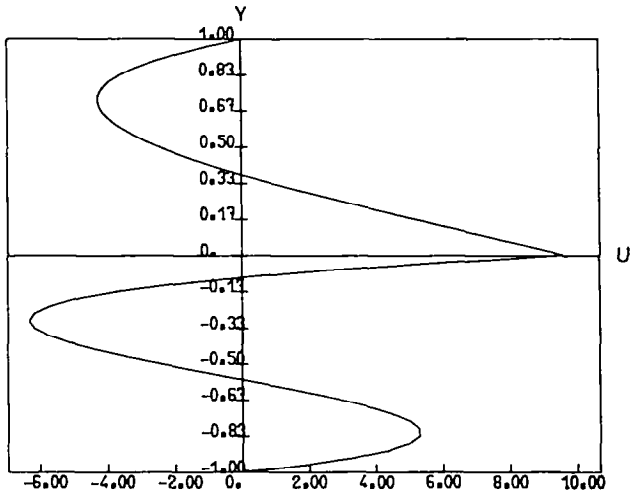

FIG. 2. Horizontal velocity profile for case A at $Gr = 10^3$, $Re_2 = -350$; $Q\alpha = 1.33$ and $Q\mu = 8.73$, $h_1 = 5.6$ and $h_2 = 3.7$.

each layer, with the same direction of rotation. The needed condition to have Pa_1 or Pa_2 equal to zero is

$$Re_2 = \left(\frac{Q\alpha - 1}{12}\right) h_2^3 \, Gr. \tag{23}$$

(2) When $0 < Pa_2/Gr < 2$, there exists two negative roots in the lower liquid and only one positive root in the upper liquid layer. Therefore, we know that there are two convective cells in liquid layer 2 and only one convective cell in liquid layer 1.

(3) When $0 < Pa_1/Gr < 2$ (which is analogous to case (2)), there exists two positive roots in the upper layer and only one negative root in the lower layer (except the roots at the upper and lower rigid walls). Consequently, there is only one cell in layer 2 and two cells in layer 1.

(4) The velocity at the interface ($y' = 0$) is positive when $Pa_2 > 0$ (or $Pa_1 < 0$) and negative when $Pa_2 < 0$ (or $Pa_1 > 0$).

3.2. *Free top surface (case B)*

Expressions of the horizontal velocity in the two layers are given here

$$u_1(y') = \frac{Gr\, h_2^3}{6}\left(\frac{Q\alpha}{Q\mu}y'^3 - \frac{1+6Q\alpha+10\dfrac{Q\alpha}{Q\mu}}{4(Q\mu+\frac{4}{3})}y'^2 + \frac{1+2\dfrac{Q\alpha}{Q\mu}}{2(Q\mu+\frac{4}{3})}y' + \frac{3Q\alpha-2}{12(Q\mu+\frac{4}{3})}\right) + \frac{h_2}{6(Q\mu+\frac{4}{3})}\left(-3\left(Re_2+\left(1+\frac{2}{Q\mu}\right)Re_1\right)y'^2 + 2\left(3Re_2+\frac{2}{Q\mu}Re_1\right)y' + (Re_1-2Re_2)\right) \tag{24}$$

$$u_2(y') = \frac{Gr\, h_2^3}{6}\left(y'^3 + \frac{3(2+2Q\mu+Q\alpha)}{4(Q\mu+\frac{4}{3})}y'^2 + \frac{Q\mu+2Q\alpha}{2(Q\mu+\frac{4}{3})}y' + \frac{3Q\alpha-2}{12(Q\mu+\frac{4}{3})}\right) + \frac{h_2(Re_1-2Re_2)}{6(Q\mu+\frac{4}{3})}(3y'^2+4y'+1). \tag{25}$$

The velocity profiles in each liquid layer depend on (Gr, Re_1, Re_2, $Q\mu$, $Q\alpha$) and are the sum of two terms. The first term is related to buoyancy force and as usual is a cubic polynomial. The second concerns thermocapillary forces and is quadratic. In a gravitational field, when $Re_1 = 2Re_2$, the velocity profiles of the lower liquid are not influenced by the surface tension gradients at the interface between the two liquids (or at the free surface of the upper liquid). In addition, the interface is at rest when $Q\alpha = 2/3$.

Without gravitation, i.e. at $Gr = 0$, the velocity profiles depend on (Re_1, Re_2, $Q\mu$) and only one convective cell appears in the lower liquid layer since there are only two roots (with one always located at the lower wall). In particular, it should be noted that no convective motion exists in the lower liquid layer when $Re_1 = 2Re_2$ (i.e. when: $\partial\sigma_1/\partial T = 2\,\partial\sigma_2/\partial T$). This condition for zero motion was previously given by Doi and Koster [11].

4. NUMERICAL SOLUTION FOR FINITE LAYERS

The complete system of the governing equations (with appropriate boundary conditions) is solved by a finite difference technique with an alternating-direction implicit (ADI) formulation to obtain a steady solution, asymptotically (i.e. for $t \to \infty$). The dependent variables (u_i, v_i, p_i, θ_i) are represented by their

values on a staggered grid [13]. We use a predictor–corrector method to decouple the pressure computation from that of the velocity and temperature [14]. This approach requires the resolution of a Poisson equation for the pressure, at each time step. For the internal nodes, the spatial derivatives are approximated by standard central differences. At the boundary, second-order accurate discretization is employed

$$\frac{\partial \phi}{\partial x} = \frac{\phi_0 - \phi_1}{0.5x} + \frac{2\phi_0 + \phi_2 - 3\phi_1}{3x}$$

where ϕ_1, ϕ_2 are internal nodes and ϕ_0 the boundary node. For the external nodes, we use the classical approximation [15]

$$\phi_{-1} = \frac{8\phi_0 - 6\phi_1 + \phi_2}{3}.$$

For spatial discretization, the number of grids in the vertical direction is $NY1$ in the upper layer and $NY2$ in the lower one. Different values of $NY1$ and $NY2$ are used for different thickness ratios of the two layers, in order to keep the accuracy.

The grid-dependency of the solution was analyzed for three uniform grids of $(21+21)\times 81$, $(31+31)\times 121$ and $(41+41)\times 161$ points for case B. There are many factors affecting the convection in two-layer systems. But, for these grid tests, we choose the simplest property ratios such as $A = 2$, $h^* = \mu^* = \alpha^* = \lambda^* = 1$, $\rho^* = 0.1$, and $\beta^* = 5$. The other chosen dimensionless parameters are: $Gr = 10^4$, $Re_1 = -150$, $Re_2 = -100$, and $Pr = 1$. The main features of solutions for different grids are presented in Table 1, for a steady solution. They concern some characteristic values such as: $u_{i_{max}}$, $v_{i_{max}}$, $u_{F_{max}}$ and $u_{I_{max}}$ $(i = 1, 2)$, where $u_{i_{max}}$ is the maximum of u_i at $x = 0.25$, $v_{i_{max}}$ is the maximum of v_1 at $y = 0.125$ and v_2 at $y = -0.125$, $u_{F_{max}}$ ($u_{F_{min}}$) is the maximum (minimum) of the velocity at free top surface and $u_{I_{max}}$ ($u_{I_{min}}$) is the maximum (minimum) of the interface velocity.

The typical CPU time required to reach a steady solution is 0.2 s per time step for a $(31+31)\times 121$ mesh and 0.35 s for a $(41+41)\times 161$ mesh. All computations are carried out in double precision on an IBM 3090-600/VF computer. The difference between the velocities obtained for a $(31+31)\times 121$ mesh and a $(21+21)\times 81$ mesh, is generally less than 4%. The difference for a $(41+41)\times 161$ mesh and a $(31+31)\times 121$ mesh is generally less than 1%; but the CPU time, per time step, increases by a factor of 75%. We finally selected the $(31+31)\times 121$ grid which gives a good compromise (enough accuracy without excessive computation time).

5. RESULTS AND DISCUSSION

In numerical simulations of convective flow in two-layer systems, both positive and negative Reynolds numbers are considered. These two opposite situations are obtained by changing the sign of surface tension gradient which fixes the direction of the thermocapillary force. It is possible to realize these different situations through the proper choice of two immiscible liquids. All the results reported below were obtained with $\mu^* = \alpha^* = \lambda^* = 1$, $\rho^* = 0.1$, and $\beta^* = 5$, and for zero heat flux through the external boundary $(y = h_1)$. This case corresponds to $Q\alpha = 0.5$ and $Q\mu = 1$, and thus $Pa_1 = -2Pa_2$.

In Figs. 3(a) and 4(a) we compare the analytical profile of horizontal velocity with the numerical results in the vertical median plane (at $x = 1$), for cases A and B, respectively. The numerical results are in good agreement with the analytical model, except that there exists a small difference near the region of the maximum (minimum) velocity, which is the result of confinement effect; the flow has not been fully accelerated in the horizontal direction. In Figs. 3(b), (c) and Figs. 4(b), (c), we present the numerical streamline and isotherm patterns, for cases A and B, respectively.

5.1. *Rigid top wall (case A)*

Five different groups of the physical parameters have been selected for showing typical convections in a rectangular cavity for two-layer systems with a constant thickness ratio of the two liquid layers ($h^* = 1$), which are driven by the buoyancy forces and the surface tension gradients created by a temperature difference imposed along a flat liquid 1–liquid 2 interface:

(1) In Fig. 3 the streamlines and the horizontal velocity profile in the mid-plane (at $x = A/2$) are shown for $Gr = 10^4$, $Re_2 = -100$ (positive $\partial\sigma_2/\partial T$) and $Pr = 1$. It corresponds to specific values of the 'stream pattern parameters' such that $Pa_1/Gr = 0.02$ $(Pa_2/Gr = -0.01)$. In this case the analytical velocity

Table 1. Solution features for case B, $Gr = 10^4$, $Pr = 1$, $Re_2 = -100$, $Re_1 = -150$ and $Bi = 0$

Number of grids $(NY1+NY2)\times NX$	$u_{i_{max}}$		$v_{i_{max}}$		$u_{F_{max}}/u_{F_{min}}$	$u_{I_{max}}/u_{I_{min}}$
	$i=1$	$i=2$	$i=1$	$i=2$		
$(21+21)\times 81$	0.7609E+1	0.1001E+2	0.7786	0.5647E+1	0.9397E+1 0	0.2310E+1 −0.2347E+1
$(31+31)\times 121$	0.7546E+1	0.1007E+2	0.7869	0.5692E+1	0.9355E+1 0	0.2288E+1 −0.2346E+1
$(41+41)\times 161$	0.7515E+1	0.1009E+2	0.7921	0.5711E+1	0.9337E+1 0	0.2283E+1 −0.2346E+1

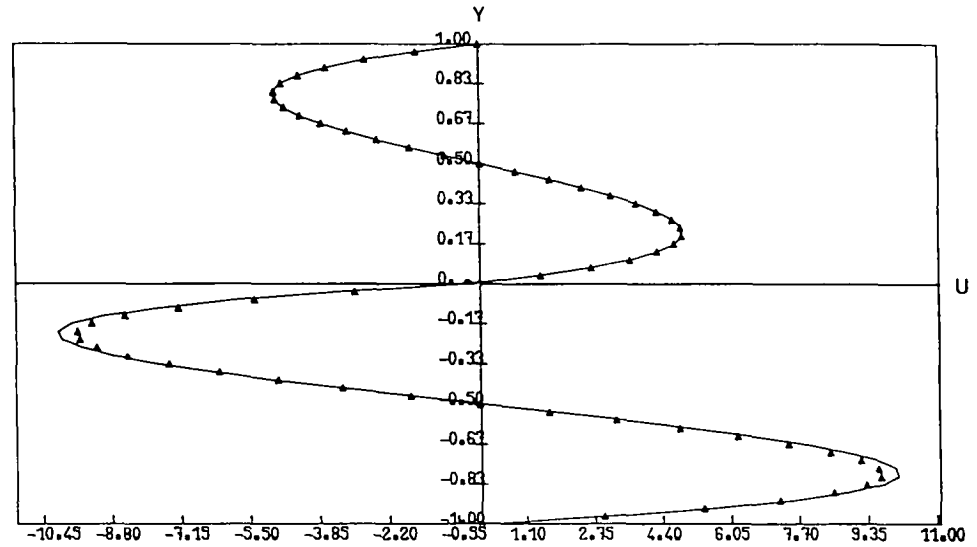

(a)

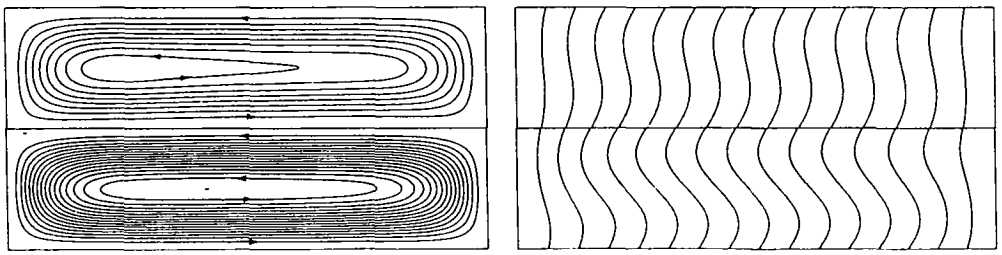

(b) (c)

FIG. 3. Characteristic results for case A at $Gr = 10^4$, $Pr = 1$, $Re_2 = -100$: (a) horizontal velocity profile on the vertical median plane; (b) streamfunction patterns, $\Psi_{max} = 1.565$, $\Psi_{min} = -0.1375 \times 10^{-1}$; (c) isotherm patterns.

at the interface is close to zero and there exists only one convective cell in layer 2 and two cells in layer 1; but, the secondary counter-rotating convective cell near the interface is very weak and thin, and cannot be seen in Fig. 3(a). Figure 5 shows that the interface velocity is also close to zero. The profile along x can be divided into three regions: with very low velocity in the central region and higher velocity near the cold and hot walls. That means that the upper cell imposes its flow direction at $y = 0$, near the end regions. When we slightly decrease Re_2 (e.g. $Re_2 = -104.2$), Pa_1 and Pa_2 vanish, and then the central region with negative velocity disappears (the velocity is positive all along the interface). The interface tension acting against buoyancy (for the lower liquid 2) strengthens the flow motion from the cold to the hot end at the interface. There exists a main vortex in upper liquid 1 driven by interfacial thermocapillary and buoyancy forces, together.

(2) To consider a case in which the thermocapillarity acts more strongly than buoyancy forces into the bulk, we decrease Gr and Pr (thus increasing Re). As an example, we take $Gr = 10^3$, $Pr = 0.1$, and $Re_2 = -1000$, leading to the following stream-pattern parameters, $Pa_1/Gr = -47.5$ ($Pa_2/Gr = 23.75$). In this case (see Fig. 6), the velocity at the interface is

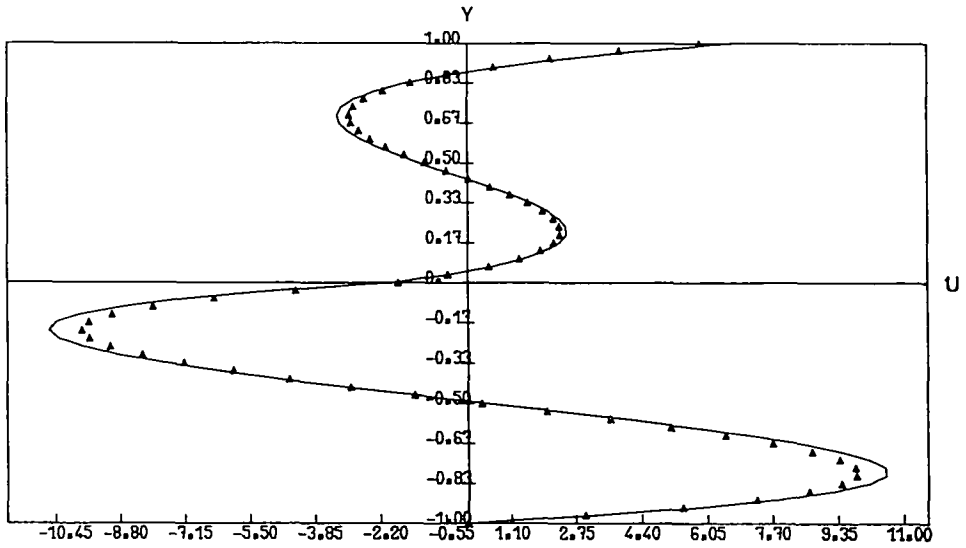

(a)

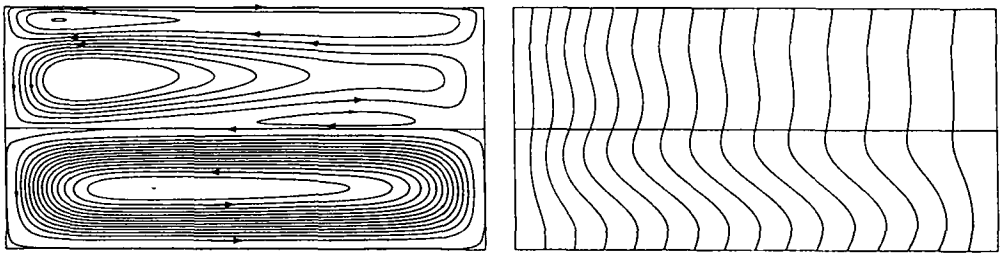

(b) (c)

FIG. 4. Characteristic results for case B at $Gr = 10^4$, $Pr = 1$, $Re_2 = -100$, $Re_1 = -150$ and $Bi = 0$: (a) horizontal velocity profile on the vertical median plane; (b) streamfunction patterns, $\Psi_{max} = 1.638$, $\Psi_{min} = -0.2321$; (c) isothermal patterns.

positive and there exists a single counter-rotative cell induced mainly by interface tension in the lower layer and a single cell induced by buoyancy (added by interface tension) in the upper layer. The horizontal velocity at the interface reaches the maximum value in the cavity mid-plane.

(3) We consider negative $\partial\sigma_2/\partial T$, which can be considered as the 'opposite' of case (2). Figure 7 presents results for $Re_2 = 1000$, where the values of stream-pattern parameters are $Pa_1/Gr = 48.5$ $(Pa_2/Gr = -24.25)$. The velocity at the interface is negative and reaches the minimum value in the entire flow field. In the liquid 1 layer the main counter-rotating cell induced by higher interfacial tension is formed and a buoyancy driven cell is not visible. In the liquid 2 layer with the interfacial tension adding buoyancy at the interface, it remains a single strong cell. We can note that a large gradient of horizontal velocity appears near the interface, in both cases (2) and (3).

(4) On the basis of case (1), we increase the thermocapillarity by taking $Re_2 = -250$ (Fig. 8), for which $Pa_1/Gr = -0.7$ $(Pa_2/Gr = 0.35)$. The results in the mid-plane are in good agreement with the prediction of infinite theoretical analysis obtained by equations (19) and (20). We can clearly find a second counter-rotating cell induced by the thermocapillary force near the interface. Under the secondary vortex, there exists a stronger convective cell induced by buoyancy forces

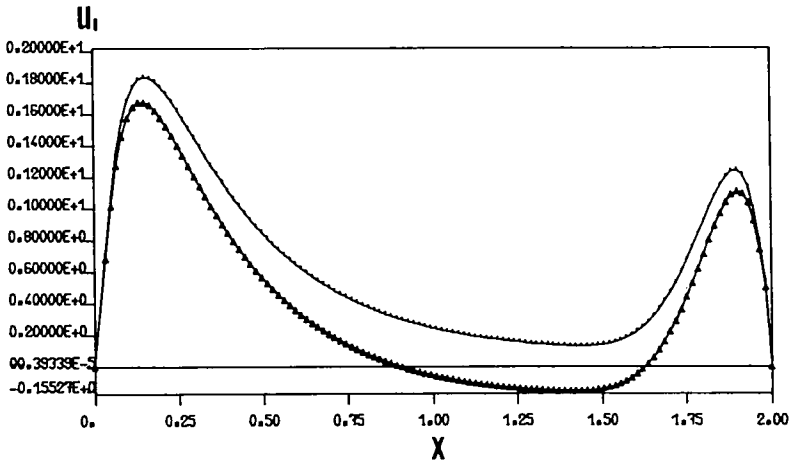

FIG. 5. Horizontal velocity profile at the liquid–liquid interface for $Gr = 10^4$ and $Pr = 1$; for $Re_2 = -100$ ($\triangle$) and $Re_2 = -104.2$ ($*$).

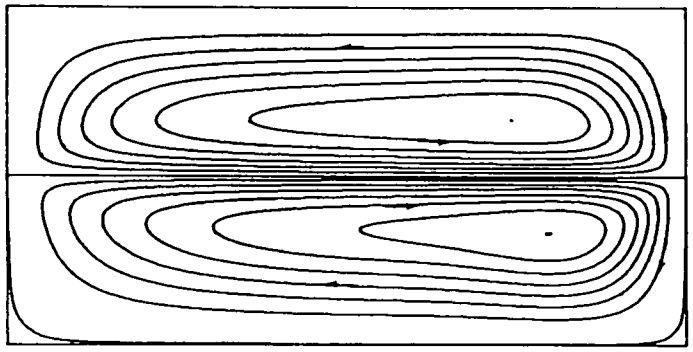

(a)

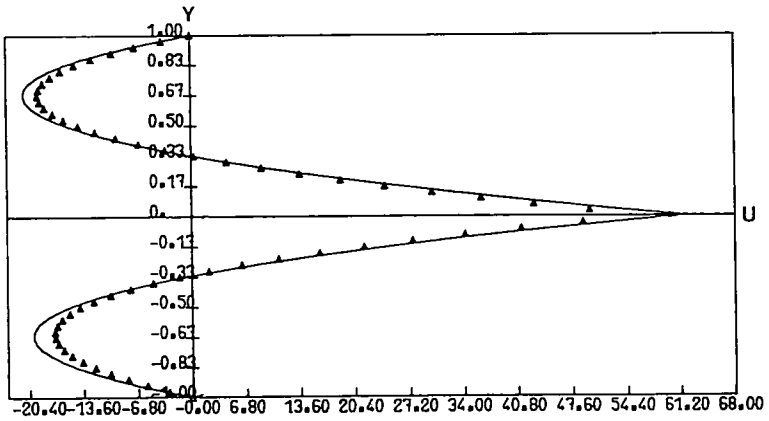

(b)

FIG. 6. Characteristic results for case A at $Gr = 10^3$, $Pr = 0.1$, $Re_2 = -1000$: (a) streamfunction pattern, $\Psi_{max} = 4.6201$, $\Psi_{min} = -4.6232$; (b) horizontal velocity profile on the vertical median plane.

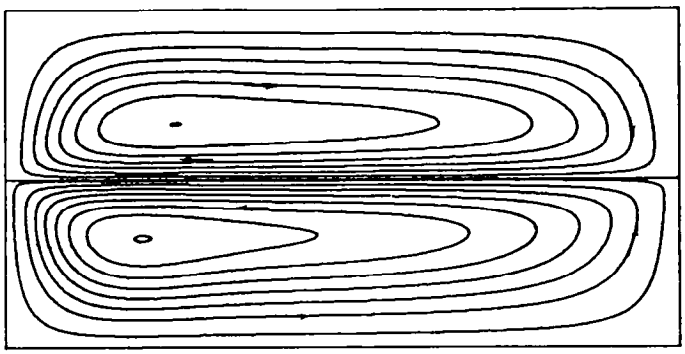

(a)

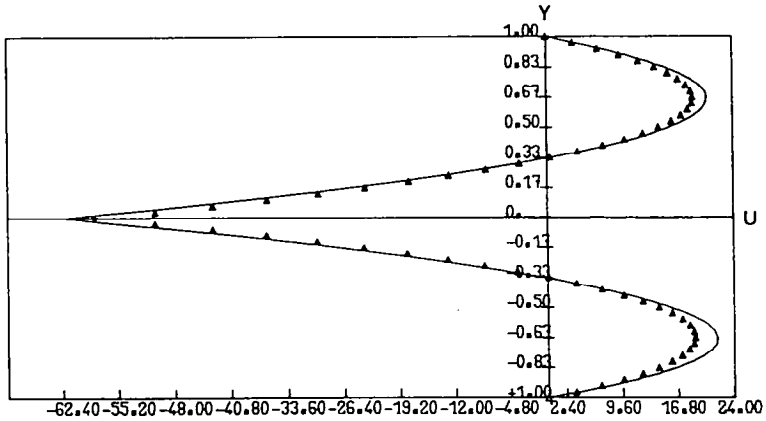

(b)

FIG. 7. Characteristic results for case A at $Gr = 10^3$, $Pr = 0.1$, $Re_2 = 1000$: (a) streamfunction patterns, $\Psi_{max} = 5.009$, $\Psi_{min} = -4.6011$; (b) horizontal velocity profile on the vertical median plane.

which has a larger size. The velocity at the interface is close to the maximum value of velocity profiles in the vertical median plane of this cavity. After the comparison with case (1), one could know that, with the augmentation of interfacial thermocapillary action, the buoyancy-driven flow in the lower layer is weakened and the flow driven by buoyancy and thermocapillarity in the upper layer is augmented.

(5) For $Re_2 = 100$ and keeping the other parameters unchanged with respect to case (1), thermocapillarity plays against buoyancy in the upper layer; its relative importance is demonstrated in Fig. 9. Beside the main tension-induced cell, the slight buoyancy-driven cell has a tendency to separate into two small vortices at the corners of the upper layer. Obviously, the maximum of velocity in liquid 1 decreases and the one in liquid 2 increases as compared with case (1).

Figure 10 shows the influence of the thickness ratio h^* of the two liquid layers for $Gr = 10^4$, $Re_2 = -100$ (case (1); see Fig. 3). When h^* is less than one (see Figs. 10(a)–(c)), the main motion occurs in the lower layer as a single cell (anti-clockwise) which is dominated by buoyancy (despite the opposition of thermocapillarity). This strong cell affects the direction of flow motion (which is clockwise) in the upper layer, for small h^*. This clockwise motion in the upper layer becomes less and less intense when h^* is increased, and finally vanishes for $h^* = 0.8$ (Fig. 10(c)); at the same moment an anti-clockwise motion, mainly induced by buoyancy, increases. This buoyancy-driven flow in the upper layer appears in the corner (Fig. 10(b)) and finally occupies all the upper layer for $h^* \geqslant 0.8$ (Figs. 10(c)–(f)). The variation of the streamfunction maximum ($\Psi_{i_{max}}$) of the anti-clockwise cells (mainly induced by buoyancy) is shown in Fig.

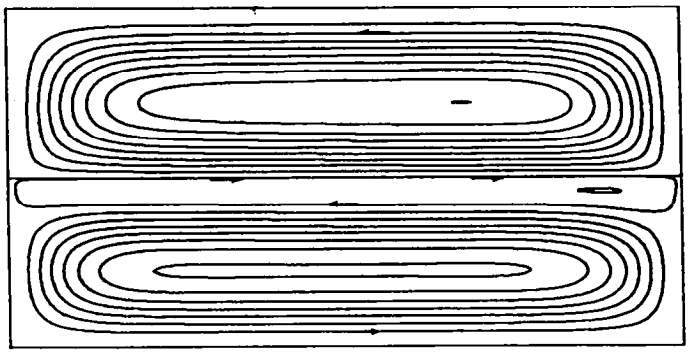

(a)

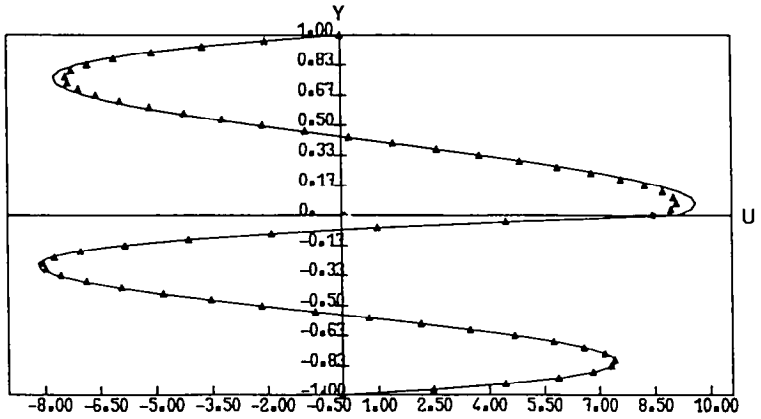

(b)

FIG. 8. Characteristic results for case A at $Gr = 10^4$, $Pr = 1$, $Re_2 = -250$: (a) streamfunction patterns, $\Psi_{max} = 1.365$, $\Psi_{min} = -0.1692$; (b) horizontal velocity profile on the vertical median plane.

11, for the two layers; $\Psi_{1_{max}}$ increases and $\Psi_{2_{max}}$ decreases with the augmentation of the thickness ratio. When h^* is greater than one (Figs. 10(d)–(f)), the change of the flow structure with increasing h^* occurs in the opposite manner. There exists only one main cell in the upper layer, jointly driven by buoyancy and thermocapillarity (negative Re_2). Then, in the lower layer, a buoyancy-cell exists at the cavity bottom (but becomes smaller and smaller), while an intermediate (clockwise) cell, induced by the upper layer flow, becomes stronger and stronger (Figs. 10(d)–(e)). In particular, two buoyancy-driven cells can be seen in the two corners of the lower layer in Fig. 10(e). A similar phenomenon has been observed in experiments with water–heptanol by Villers and Platten [16]. For higher h^*, the buoyancy cells vanish and the clockwise cell occupies the entire lower layer (Fig. 10(f)).

5.2. *Free top surface (case B)*

An example of two immiscible liquids with free top surface is presented in Fig. 4, for $h^* = 1$, and for $Gr = 10^4$, $Re_2 = -100$, $Re_1 = -150$ and $Pr = 1$. As compared with case A (Fig. 3), a secondary clockwise cell appears near the free top surface due to thermocapillary forces, while the structure of flow fields in the lower layer is almost unchanged. In addition, we observe a third intermediate (clockwise) cell existing in the upper layer, near the interface, induced by the two main anti-clockwise cells generated by buoyancy in the upper and lower layers. Thus, the motion in two superposed liquid layers appears to be more complicated for the free than for the rigid top surface.

The influence of thickness ratio on flow structure is shown in Fig. 12 (similar to Fig. 10, for case A). When the top surface is free, the flow configuration in layer 2 is almost unchanged, but layer 1 presents obvious

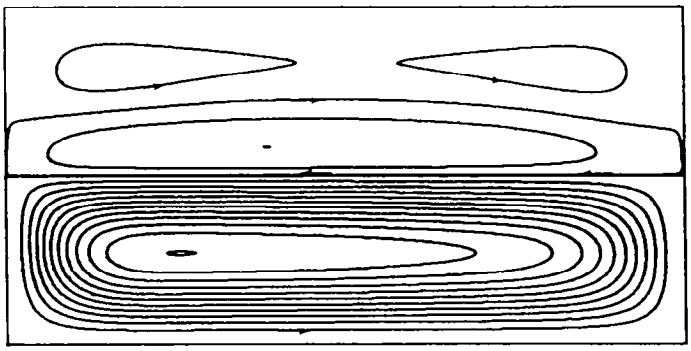

(a)

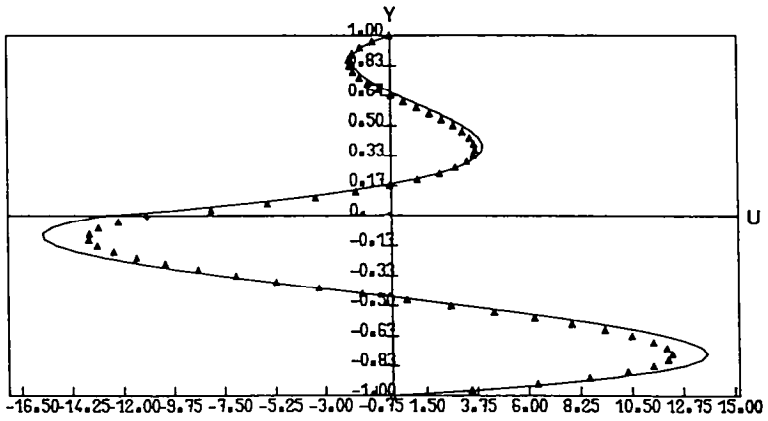

(b)

FIG. 9. Characteristic results for case A at $Gr = 10^4$, $Pr = 1$, $Re_2 = 100$: (a) streamfunction patterns, $\Psi_{max} = 0.2231 \times 10^2$, $\Psi_{min} = -0.4077$; (b) horizontal velocity profile on the vertical median plane.

changes. The strength of the buoyancy cell in the lower layer augments with the decrease of thickness ratio, h^*, and the liquid at the interface moves from the hot end to the cold end walls, except near these end walls. Thermocapillarity on the free top surface overcomes buoyancy and forces the liquid to flow from the cold end to the hot end at the top surface. The buoyancy leads to two small vortices placed at the corners near the top surface; these vortices decrease rapidly both in amplitude and in size with the decrease of thickness ratio. When $h^* = 0.2$ in Fig. 12(a), the gravitational convection in liquid 1 almost vanishes. The convective cell induced by thermocapillary forces on the upper boundary and by the action of the lower liquid layer through the interface is always dominant in liquid 1. When $h^* > 1$ (Figs. 12(c) and (d)), the gravitational convection dominates in layer 1 and intensifies with the increase of h^*. The obvious difference from case A is that there exists a smaller clockwise vortex, driven by thermocapillary force, in the left-upper corner of liquid 1, where large gradients of surface temperature, $\partial\theta/\partial x$, produced by convective flow, induce strong changes in the surface tension (σ_1) against buoyancy convection. This thermocapillary-vortex seems to not vanish even for larger h^*.

In order to study the combined effect of surface tension gradients at the interface and free top surface, we consider two combinations of the Reynolds numbers, Re_1 and Re_2, such that $Re_1 = 2Re_2$ (case I) and $2Re_1 = Re_2$ (case II). Investigations have been made for a particular example where $Q\alpha = 2/3$, for which the interface velocity of an infinite layer is zero for case I (after equations (24) and (25)). The other chosen physical parameters are: $Gr = 10^4$, $h^* = \alpha^* = \mu^* =$

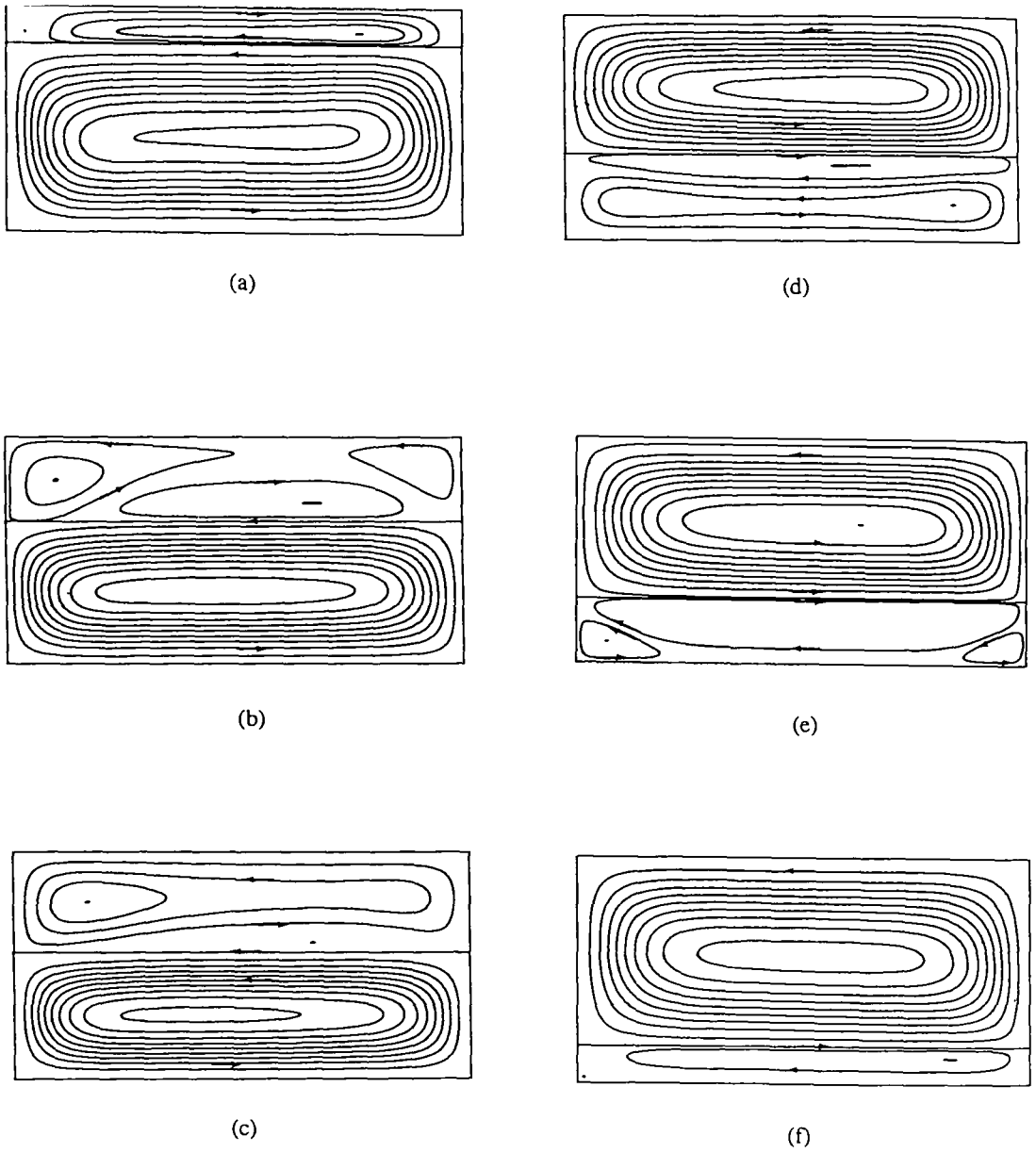

FIG. 10. Depth fraction effect on the streamlines (case A), for $Gr = 10^4$, $Re_2 = 100$ and $Pr = 1$: (a) $h^* = 0.2$; (b) $h^* = 0.6$; (c) $h^* = 0.8$; (d) $h^* = 1.6$; (e) $h^* = 2.5$; (f) $h^* = 5$.

$\lambda^* = 1$, $\rho^* = 0.1$, $\beta^* = 20/3$ and a low Prandtl number: $Pr = 0.01$ (e.g. liquid metals).

Case I ($Re_1 = 2Re_2 = 8 \times 10^4$)

We display in Fig. 13 the minimum value of horizontal velocities at interface, $u_{1_{min}}$, and at the free top surface, $u_{F_{min}}$, for $Re_1 = 2Re_2 = 8 \times 10^4$ and $Gr = 10^4$. The liquids at the interface and the free surface move from the hot end to the cold end of the cavity with positive Reynolds numbers and their values are negative in our coordinate system. The minimum value of the velocity at the interface is much less than the one at the top surface, but is not zero, as predicted by the analytical method (equations (24) and (25)). The analytical velocities at the top surface are larger than the numerical results, since the flow is not fully developed in the two-dimensional case, in particular at high Reynolds numbers [17].

Streamlines for $Re_1 = 2Re_2 = 8 \times 10^4$ and the corresponding variation of the horizontal velocity, u_F, along the top surface and u_1, along interface between two liquids are presented in Fig. 14. The lower layer exhibits a cell (the center of which is placed near the cold wall), but the fluid moves very slowly near the bottom. The flow structure mainly depends upon thermocapillary forces along the top surface and inter-

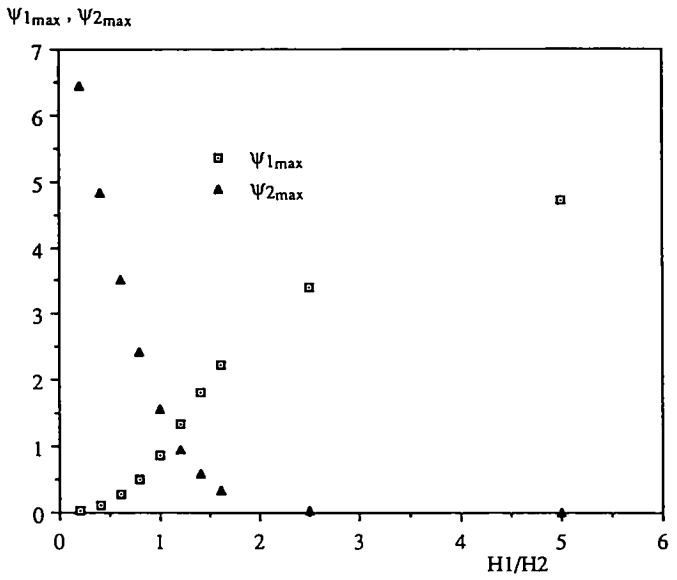

FIG. 11. Variation of the maximum streamfunction as a function of h^*, for $Gr = 10^4$, $Re_2 = -100$ and $Pr = 1$.

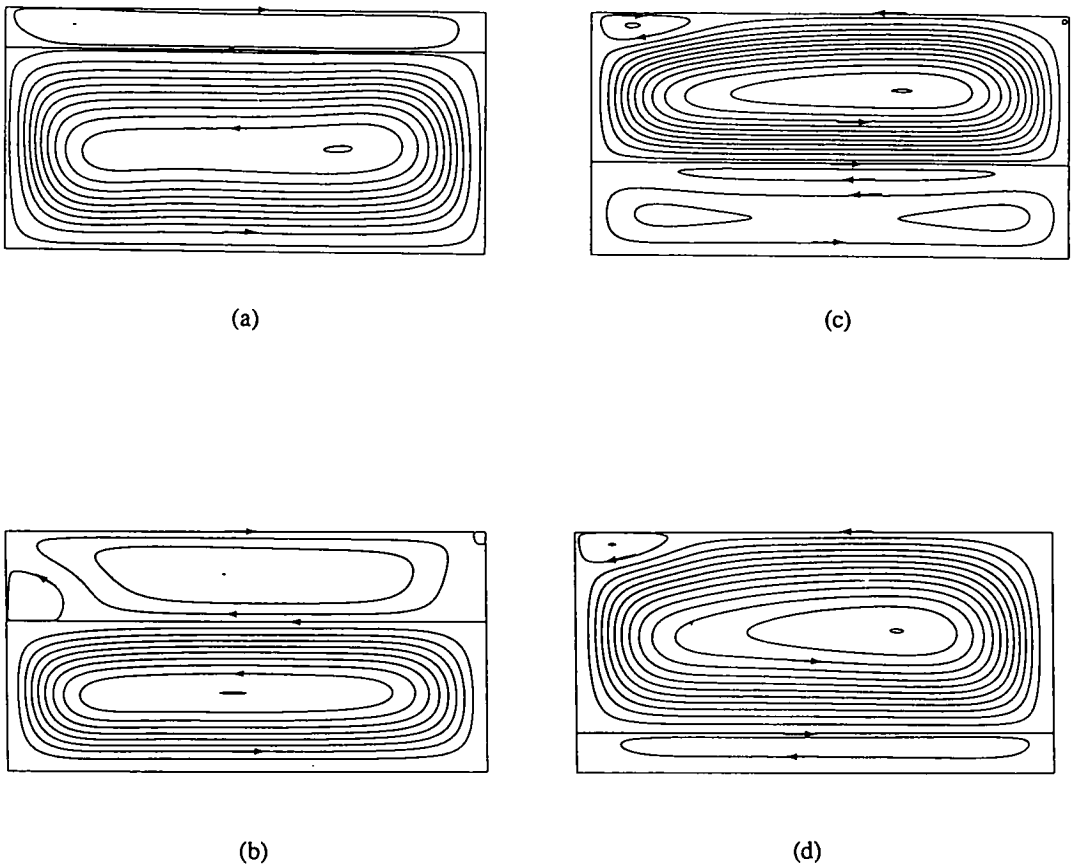

FIG. 12. Depth fraction effect on the streamlines (case B), for $Gr = 10^4$, $Re_2 = -100$, $Re_1 = -150$, $Bi = 0$ and $Pr = 1$: (a) $h^* = 0.2$, $\Psi_{max} = 6.011$, $\Psi_{min} = -0.4949$; (b) $h^* = 0.6$, $\Psi_{max} = 3.536$, $\Psi_{min} = -0.8794$; (d) $h^* = 1.6$, $\Psi_{max} = 2.117$, $\Psi_{min} = -0.2882$; (g) $h^* = 5$, $\Psi_{max} = 4.607$, $\Psi_{min} = -0.4439$.

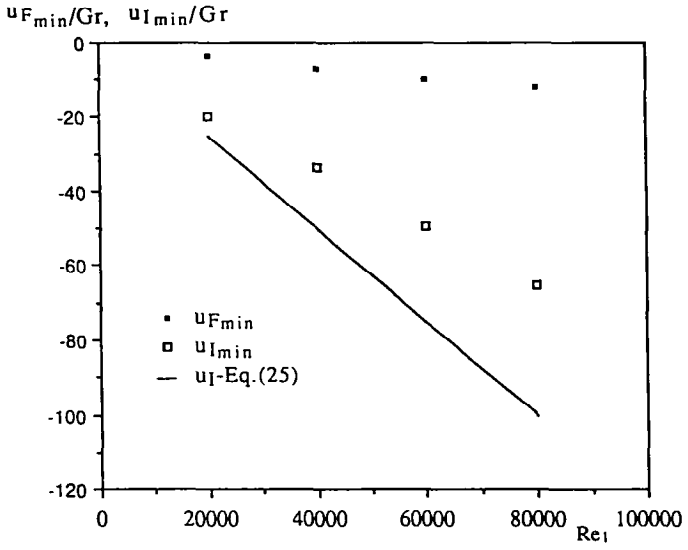

FIG. 13. Minimum velocities at interface (case B), for different Reynolds numbers such that $Re_1 = 2Re_2$, for $Gr = 10^4$ and $Pr = 0.01$.

(a)

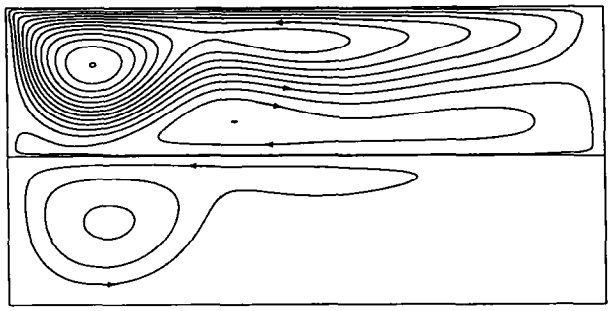

(b)

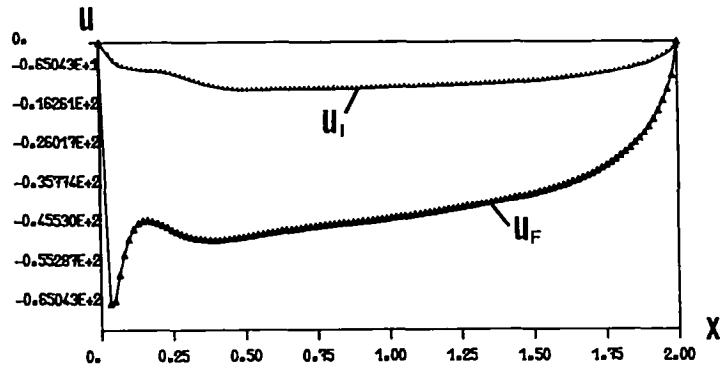

FIG. 14. Characteristic results for $Gr = 10^4$, $Pr = 0.01$, $Re_1 = 2Re_2 = 8 \times 10^4$: (a) streamfunction patterns, $\Psi_{max} = 3.8117 \times 10^2$, $\Psi_{min} = -0.6864 \times 10^2$; (b) horizontal profiles at the free top surface U_F and at the liquid–liquid interface U_I.

face, and the effect of gravity forces is weak (relative to the thermocapillary force).

The numerical results show that the maximum value of streamfunction in the upper layer, $\Psi_{1_{max}}$, increases much more rapidly than $\Psi_{2_{max}}$, in the lower layer, when the Reynolds number is increased.

Case II ($Re_2 = 2Re_1 = 8 \times 10^4$)

Here, we show in Fig. 15(a) the minimum velocities at the interface and free top surface for $Re_2 = 2Re_1 = 8 \times 10^4$ and $Gr = 10^4$. These two specific velocities are close to each other and differ from the analytical velocities of the infinite layer for higher Reynolds number. Note that the flow structure (Fig. 15(b)) in the lower layer is more complex; a clockwise intermediate cell in the upper has grown in intensity and size (reaching the end walls), near the interface where the thermocapillary effect has been greatly increased, compared to case I. The cell in the lower layer has augmented rapidly in intensity with the increase of Re_2.

In the above comparative simulation, we could observe that there exists a significant damping effect of convection in the upper layer on the motion in the lower layer, for a proper choice of the parameters, in particular when $Re_1 = 2Re_2$. The thermocapillary force on the top surface has been shown to overcome that on the interface, even for $Gr = 10^4$. Then, under the microgravity conditions ($Gr \to 0$), the thermal convective flow in liquid 2 would be very weak since buoyancy forces are absent.

6. CONCLUSION

We have shown in this paper some typical convection patterns in the case of two superposed immis-

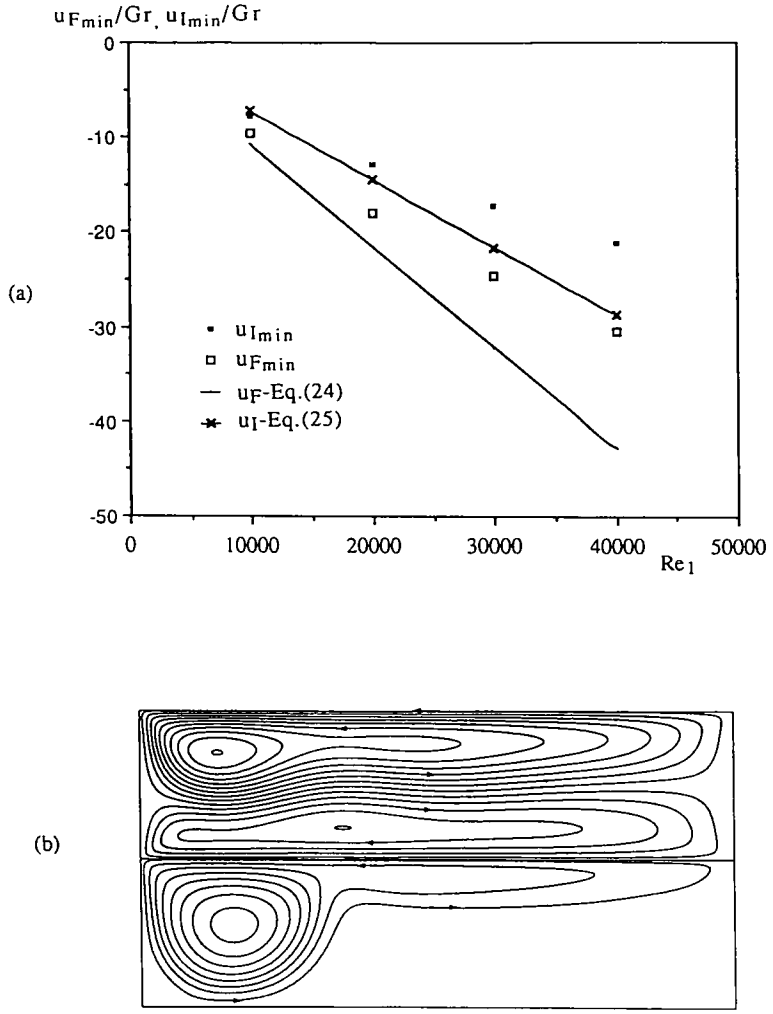

FIG. 15. Characteristic results $Re_2 = 2Re_1 = 8 \times 10^4$ (in case B) for $Gr = 10^4$ and $Pr = 0.01$: (a) minimum velocities at two interfaces for different Reynolds numbers, $\Psi_{max} = 1.8624 \times 10^2$, $\Psi_{min} = -0.8981 \times 10^2$; (b) streamfunction patterns.

cible liquid layers, which are induced not only by density differences in the gravitational field, but also by interfacial tension gradients. Under the coupling of buoyancy and thermocapillary convections, the flow structures always have an obvious change in the regions near the interface when some parameters are changed. An interfacial convective cell is frequently displayed either in the upper layer or in the lower layer, in order to satisfy continuity of velocity and stress balance at the interface. The position and relative size of this cell depends on various parameters, such as expansion coefficient, viscosity, thickness of each liquid layer. When the thickness or the buoyancy force decreases in one of the two phases, the interfacial tension plays a major role. The flow at the interface and in each of the two layers can be significantly controlled by a proper choice of physical parameters.

This paper is just a preliminary investigation. The free surface was taken here as underformable so that numerical results could be compared to analytical solutions for infinite layers. A more detailed and quantitative investigation of two-layer systems should be made in the near future by considering interface deformation as well as the stability of the system, in particular, for thermocapillary convection under microgravity conditions.

Acknowledgements—This investigation was supported by the Centre National d'Etudes Spatiales (Divison Fluides et Matériaux en Microgravité). The computations were carried out on IBM3090-600/VF of CNUSC.

REFERENCES

1. Y. Renardy and D. D. Joseph, Oscillatory instability in Bénard problem of two fluids, *Physics Fluids* **28,** 788–793 (1985).
2. R. W. Zeren and W. C. Reynolds, Thermal instabilities in two-fluid horizontal layers, *J. Fluid Mech.* **53,** 305–327 (1972).
3. G. Z. Gershuni and E. M. Zhukhovitsky, On instability of equilibrium of the system of horizontal layers of immiscible fluids when heated from above, *Common Acad. Sci. URSS, Mech. Fluids Gases* **6,** 28–34 (1980).
4. G. Z. Gershuni and E. M. Zhukhovitsky, On monotonoms and oscillative instability of two-layer system of immiscible fluids when heated from below, *Rep. Acad. Sci. URSS* **265,** 302–305 (1982).
5. Y. Renardy and D. D. Joseph, Instability at the interface between two shearing fluids in a channel, *Physics Fluids* **28,** 3441–3443 (1985).
6. A. P. Hooper, Long-wave instability at the interface between two viscous fluids: thin layer effects, *Physics Fluids* **28,** 1613–1618 (1985).
7. S. Wahal and A. Bose, Rayleigh–Bénard and interfacial instabilities in two immiscible liquid layers, *Physics Fluids* **31,** 3502–3510 (1988).
8. W. H. Langlois, Buoyancy-driven flows in crystal-growth melts, *Ann. Rev. Fluid Mech.* **17,** 191–215 (1985).
9. D. Villers and J. K. Platten, Influence of interfacial tension gradients on thermal convection in two superposed immiscible liquid layers, *Appl. Scient. Res.* **47,** 177–191 (1990).
10. E. Crespo del Arco, G. P. Extremet and R. L. Sani, Thermocapillary convection in a two-layer fluid system with flat interface, *Adv. Space Res.* **11**(7), 129–132 (1991).
11. T. Doi and J. Koster, Marangoni convection in two immiscible liquid layers subject to a horizontal temperature gradient. In *Proc. 7th Int. Conf. on Physico-Chemical Hydrodynamics*, MIT, Cambridge, Massachusetts (1989).
12. C. H. Wang, M. Sen and P. Vasseur, Analytical investigation of Bénard–Marangoni convection heat transfer in a shallow cavity filled with two immiscible fluids, *Appl. Scient. Res.* **48,** 35–53 (1991).
13. F. Harlow and J. Welch, Numerical calculation of time-dependent viscous incompressible flow of fluid with free surfaces, *Physics Fluids* **8,** 2181–2189 (1965).
14. G. Chen and B. Roux, Analytical solution and numerical simulation of thermocapillary convection in floating zones, *Adv. Space Res.* **11**(7), 151–162 (1991).
15. R. Peyret and T. D. Taylor, *Computational Methods for Fluid Flows*, Springer Series in Comp. Phys. (1983).
16. D. Villers and J. K. Platten, Thermal convection in superposed immiscible liquid layers, *Appl. Scient. Res.* **45,** 145–151 (1988).
17. H. Ben Hadid and B. Roux, Thermocapillary convection in long horizontal layers of low-Prandtl-number melts subject to a horizontal temperature gradient, *J. Fluid Mech.* **221,** 77–103 (1990).